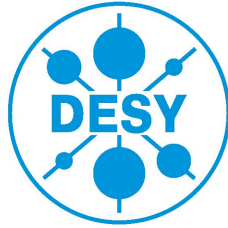


# DESY SUMMER STUDENT PROJECT 2015

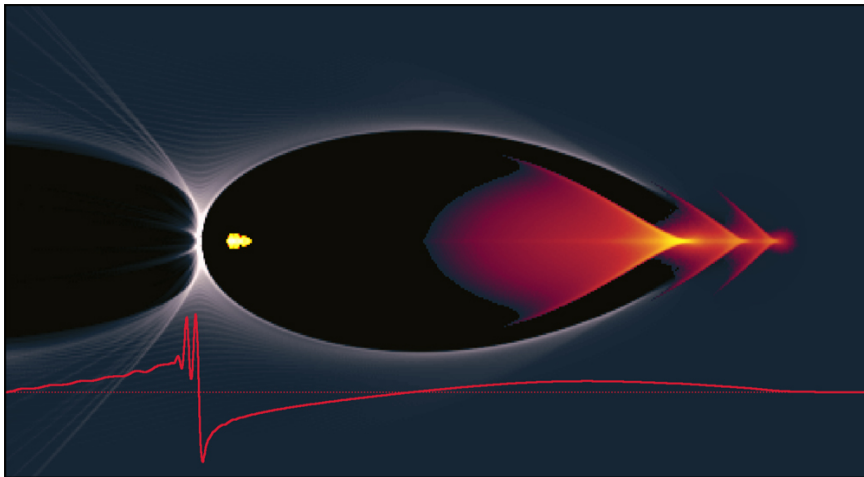


## Development of a transition radiation spectrometer for the diagnosis of ultra-short electron bunches at FLASHForward

**Silvia Seidlitz**  
(Heidelberg University)

*Research group:*  
Forschung Linear Accelerator (FLA)

*Supervisor:*  
Charlotte Palmer



Femtosecond electron bunch in a beam-driven plasma wakefield [5]

# Contents

<b>1</b>	<b>Introduction</b>	<b>3</b>
1.1	Coherent transition radiation . . . . .	3
1.2	Current situation and direction of development . . . . .	4
1.2.1	Coherent Radiation Intensity SPectrometer CRISP4 . . . . .	4
1.2.2	Double-prism spectrometer . . . . .	4
1.2.3	Two-stage prism spectrometer . . . . .	5
<b>2</b>	<b>Design of complementary grating stages</b>	<b>6</b>
2.1	Basics: How the grating works . . . . .	6
2.2	Grating design procedure . . . . .	7
2.3	Results . . . . .	8
2.3.1	Evaluation of the applicability of the stocked grating . . . . .	8
2.3.2	Commercially available gratings . . . . .	8
2.4	The focusing optics . . . . .	13
<b>3</b>	<b>Two-stage prism spectrometer: Characterization of beam splitters and measurement of visible and near-infrared TR</b>	<b>15</b>
3.1	Choice of prisms and setup parameters . . . . .	16
3.2	Alignment of the two-stage prism spectrometer . . . . .	19
3.3	Wavelength calibration . . . . .	19
<b>4</b>	<b>Further work</b>	<b>20</b>
<b>5</b>	<b>Appendix: A brief guide to zemax</b>	<b>21</b>

# 1 Introduction

Monochromatic light sources, featuring high brilliance and coherence, are of great interest in research. Their applicability is diversified over various fields including for example biology, chemistry or material science. Due to the absence of an active medium, free-electron lasers (FELs) offer important advantages compared to conventional lasers such as a high level of average power and a great tunability of the operating frequency.

In a FEL, a highly energetic beam of electrons passes through a periodic magnetic structure. The deviation of the electrons from the straight path results in the emission of synchrotron radiation. Provided sufficiently strong radiation is generated, the transverse electric field of the radiation beam interacts with the transverse electron current created by the periodical electron motion. The result is a bunching of the electrons on the scale of the radiation wavelength, causing the coherent emission of the radiation.

The high-gain operation of FELs requires sufficiently high peak currents. This is realized by longitudinal compression of the electron bunches down to sub-picosecond lengths. It is important to control this bunch compression through adjustment of the machine in order to achieve the required result. Furthermore, single shot measurements are desired due to fluctuations of machine adjustments.

A possibility to monitor the longitudinal profile of relativistic electron bunches is given by the detection of emitted coherent transition radiation (CTR) as the spectral constitution correlates with the spatial distribution within the bunch. The spectrum of this THz and infrared radiation is extremely broad and a spectrometer for bunch diagnostics covering a wavelength range from 5-44  $\mu\text{m}$  and 45-430  $\mu\text{m}$  has already been realized at the X-ray free-electron laser FLASH [1, 7]. In addition a high sensitivity double prism spectrometer covering the wavelength range 2 – 15  $\mu\text{m}$  is in use [2]. Since reconstructing the longitudinal charge distribution from CTR requires the measurement over a wide wavelength region, the aim of my summer student project was to develop and realize extensions for this spectrometer so that wavelengths down to 350  $\text{nm}$  may be reached.

## 1.1 Coherent transition radiation

Transition radiation is generated whenever a charge crosses the interface between two materials featuring different dielectric constants (figure 1).

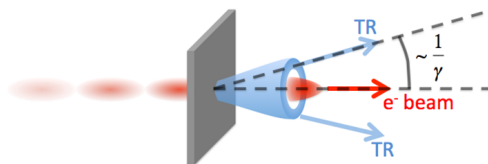


Figure 1: Generation of TR [6]

The spectrum obtained for a single charge is broad and approximately flat. For a bunch of charges, transition radiation adds coherently for wavelengths longer than the bunch length. For this so called CTR, the spectral intensity scales with the form factor<sup>1</sup>.

It is therefore possible to obtain the absolute magnitude of the form factor via measurement of the CTR intensity spectrum. Subsequently inverse Fourier transformation allows the determination of the longitudinal shape of the bunch. Indeed, inverse Fourier transformation also demands knowledge of the phase which cannot be measured by the use of a spectrometer.

The phase might be reconstructed from the radiation spectrum by applying the Kramers-Kronig dispersion relation<sup>2</sup> which requires measurements over a sufficiently large wavelength range. Thus results the necessity of a broadband spectrometer.

## 1.2 Current situation and direction of development

### 1.2.1 Coherent Radiation Intensity SPectrometer CRISP4

The setup of the pre-existing spectrometer CRISP4 is displayed in figure 2.

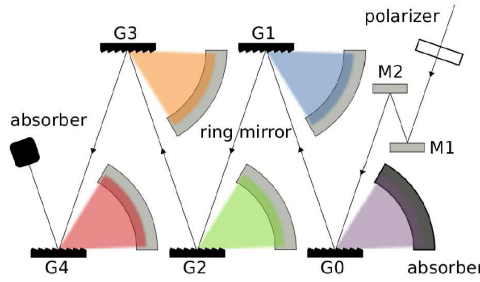


Figure 2: Setup of CRISP4 [1]

It consists of five staged reflective blazed gratings which are designed to fulfill two important functions: They act as a beam splitter transmitting CTR above a characteristic wavelength  $\lambda_c$ , with high efficiency, to the following grating situated in the zeroth order whereas wavelengths smaller than  $\lambda_c$  are, with high efficiency, diffracted into the first order and spatially separated. The diffracted light is focused on pyroelectric detectors by the use of parabolic ringmirrors [1].

### 1.2.2 Double-prism spectrometer

A double-prism spectrometer covering the wavelength range  $2 - 18 \mu m$  has been developed by S. Wunderlich [2]. It consists of two consecutive  $ZnSe$  prisms which achieve an integrated linear dispersion onto a line array of 128 mercury cadmium telluride (MCT)

<sup>1</sup>Fourier transformation of the line charge density

<sup>2</sup>Detailed explanation given in [8]

detectors (figure 3). In order to achieve a high signal-to-noise ratio, the MCT photoconductive detectors are cooled with liquid nitrogen.

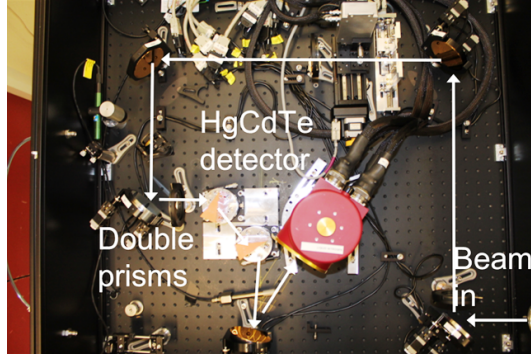


Figure 3: Setup of the double-prism spectrometer [2]

At present, it is not possible to perform measurements with CRISP4 and the double-prism spectrometer at the same time. A cascading of both spectrometers is impossible due to the TR dispersion from the double-prism spectrometer. In order to obtain a TR beam forwarded to CRISP4 and another one forwarded to the double-prism spectrometer, the placement of a beam splitter at the beginning of the setup would be required. This beam splitter would have to act over the whole wavelength range  $2 - 430 \mu m$ .

An alternative method to extend the TR spectrum towards smaller wavelengths might consist in the development of additional grating stages for CRISP4. During my summer student project, I developed a proposal for such a setup acting on the wavelength range  $1.5 - 5.2 \mu m$ .

### 1.2.3 Two-stage prism spectrometer

A two-stage prism spectrometer covering visible and near-infrared parts of the spectrum has been designed by Michael Bornholdt [3]. A schematic of the spectrometer is included in figure 4.

$P1$  was planned to measure over  $0.7 - 1.7 \mu m$ ,  $P2$  to measure over the range  $0.35 - 1 \mu m$ . Mirror  $M2$  was designed to be shiftable as this facilitates the exchange of the beam splitter. This will allow the characterization of different beam splitters using the spectrometer.

I realized parts of the prism spectrometer setup during my summer student project.

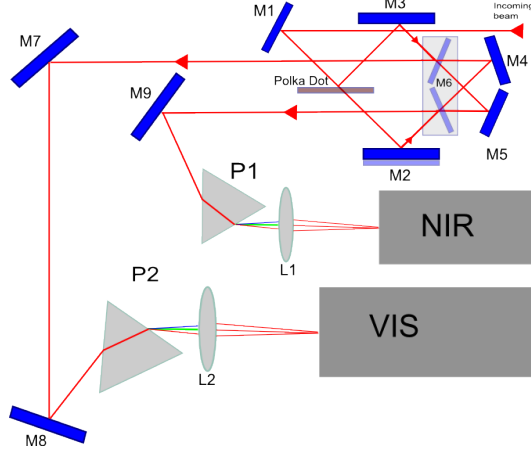


Figure 4: Setup of the two-stage prism spectrometer [3]

## 2 Design of complementary grating stages

### 2.1 Basics: How the grating works

The blazed reflection gratings feature a sawtooth shaped cross section as visible in figure 5.

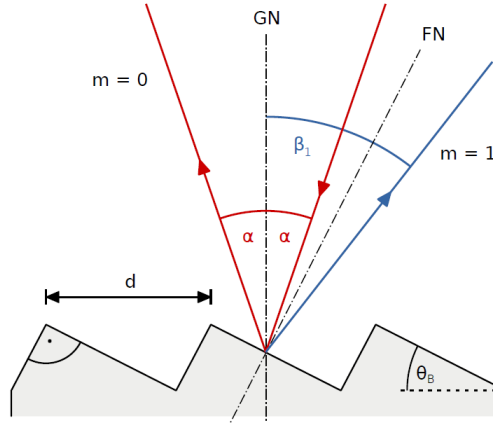


Figure 5: Cross section of a blazed grating [1]

The grating is characterized by three parameters: Line spacing  $d$ , angle of incidence  $\alpha$  and Blaze angle  $\Theta_B$ . The line spacing determines the wavelength splitting according to the diffraction equation in order  $m$

$$\sin(\alpha) + \sin(\beta_m) = \frac{m\lambda}{d}. \quad (1)$$

$\Theta_B$  is designed in order to improve the reflection efficiency for a certain wavelength range diffracted into the first order. It is intuitive that for a certain wavelength, efficiency becomes maximal when the angle enclosed with the facet normal (FN) of incident and

diffracted light are identical. In this so called Littrow configuration, the first order diffraction of the design wavelength  $\lambda_{DWL}$  fulfills

$$\Theta_B - \alpha = \beta(\lambda_{DWL}) - \Theta_B. \quad (2)$$

In the following, I will evaluate the applicability of a stocked grating featuring a groove density of 830 *lines*/ $\mu m$  and Blaze angle  $\Theta_B = 19^\circ 23'$  for my purpose and investigate gratings which might cover about 1.5–5.2  $\mu m$ . The overlap with the already measurable wavelength ranges is desired in order to facilitate the assembling.

## 2.2 Grating design procedure

The following conditions should be fulfilled:

- The first order reflection efficiency should feature a sharp bandwidth with the desired start wavelength  $\lambda_s$  and cutoff  $\lambda_c$ . The efficiency should be high over the whole bandwidth. A minimum value of 50% is proposed.
- Above  $\lambda_c$  the light should be reflected with high efficiency into the zeroth order as this light is transmitted to the following grating stage. A minimum value of 90% is proposed.
- Some limits are due to the focusing on detector: The angle of dispersion between  $\lambda_s$  and  $\lambda_c$  should not be too large because the foci form a curved line. For a small angle between the dispersed spectrum, an approximation by a flat line is possible whereas a big angle would require a curved detector. Furthermore,  $\beta(\lambda_s)$  should be larger than the angle of incidence  $\alpha$  to avoid overlapping between incident and first order diffracted radiation and allow the placement of a focusing mirror.
- The gratings should be commercially available to minimize the costs. Therefore, only reflective blazed gratings provided by thorlabs, Edmund optics and Richardson Gratings are considered.

This results in some simplified design equations:

The maximal wavelength diffracted into the first order features a diffraction angle  $\beta(\lambda_c) = 90^\circ$ . Applied on equation (1), this leads to

$$\frac{\lambda_c}{d} = \sin(\alpha) + 1 \quad (3)$$

As  $\beta(\lambda_s) > \alpha$  should be fulfilled, one can as well deduct from equation (1)

$$\frac{\lambda_s}{d} > 2 \sin(\alpha) \quad (4)$$

An equation for the Blaze angle  $\theta_B$  can be obtained from equation (2) considering that the design wavelength should be in the middle of the spectrum:

$$\lambda_{DWL} = \frac{\lambda_s + \lambda_c}{2}. \quad (5)$$

## 2.3 Results

It is impossible to achieve sufficiently small dispersion angles as well as high spectral resolution by a single grating stage covering  $1.5 - 5.2 \mu m$ . Therefore, several gratings are designed covering consecutive parts of the spectrum. A first split is proposed at  $2.1 \mu m$  regarding the available detectors:

Above  $2 \mu m$ , pyroelectric detectors might be convenient as they are robust, feature high and approximately constant sensitivity over a wide wavelength range, short response times and do not require cooling [9]. In the wavelength range  $1.5 - 2.1 \mu m$ , an InGaAs photodiode, Andor iDus 2.2, features high detection efficiency and thus is proposed to be employed to detect the TR dispersed from grating stage G1.

As the wavelength range  $2.2 - 5.2 \mu m$  still remains too large to be covered by a single grating, it is splitted into two equal parts. Grating G2 should cover  $2.2 - 3.7 \mu m$ , Grating G3 should act on  $3.8 - 5.2 \mu m$ .

### 2.3.1 Evaluation of the applicability of the stocked grating

The stocked grating features a groove density of  $830 \text{ lines}/\mu m$  and the Blaze angle  $\Theta_B = 19^\circ 23'$ . The producer declares its active wavelength range to be  $0.7 - 1.1 \mu m$ . Following equation (3), it is possible to achieve  $\lambda_c = 2.1 \mu m$  by choosing the angle of incidence  $\alpha = 49^\circ$ . However, applying equation (4), this leads to the lower limit of the detectable spectrum  $\lambda_s = 1.9 \mu m$ .

As the lower edge of the usable bandwidth of the stocked grating is considerably higher than the target value  $1.5 \mu m$ , I propose to choose an alternative grating which has been found to be more suitable for this application.

### 2.3.2 Commercially available gratings

By use of the three design equations (3) - (5), design parameters for possible gratings G1-G3 are obtained. They are listed in table 1.

Grating	$1/d \text{ [} 1/\mu m \text{]}$	$\theta_B \text{ [}^\circ \text{]}$	$\alpha \text{ [}^\circ \text{]}$
G1	0.625	36.3	18
G2	0.351	32.4	17
G3	0.282	40.5	28

Table 1: Design parameters for possible gratings



These design parameters are compared to commercially available gratings. Possible gratings which fit the closest to those parameters are listed in table 2. The angle of incidence  $\alpha$  is chosen to fulfill the desired cutoff.

Grating	Product Nb.	$1/d$ [ $1/\mu m$ ]	$\theta_B$ [ $^\circ$ ]	Length x width [mm]	$\alpha$ [ $^\circ$ ]
G1	Richardson 53-*-132R	0.600	34.0	102 x 102	15
G2	Richardson 53-*-780R	0.300	26.7	154 x 206	7
G3	Richardson 53-*-179R	0.245	36.5	158 x 208	16

Table 2: Commercially available gratings most closely resembling the design parameters

For the final configuration parameters from table 2, the first and zero order reflection efficiency spectra are computed using the commercial code PCGrate. PCGrate approximately calculates the efficiency of the diffraction grating applying the modified integral method. This method reduces the diffraction problem to solving a system of boundary equations. Figures 6-8 contain the results.

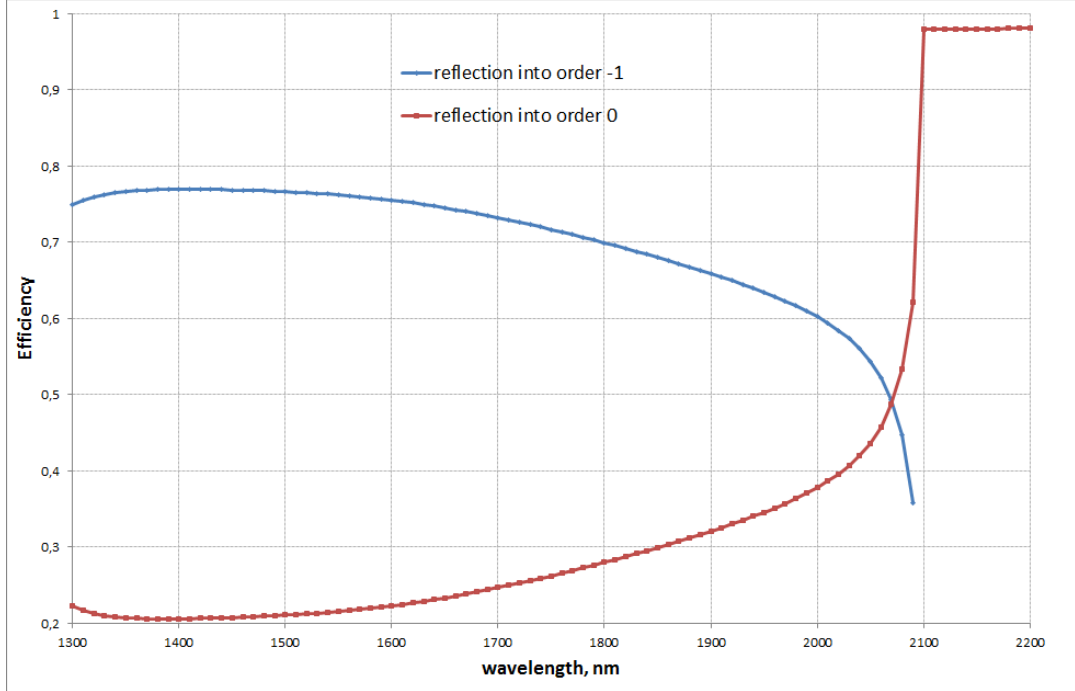


Figure 6: Efficiency spectrum of G1 with system parameters from table 2

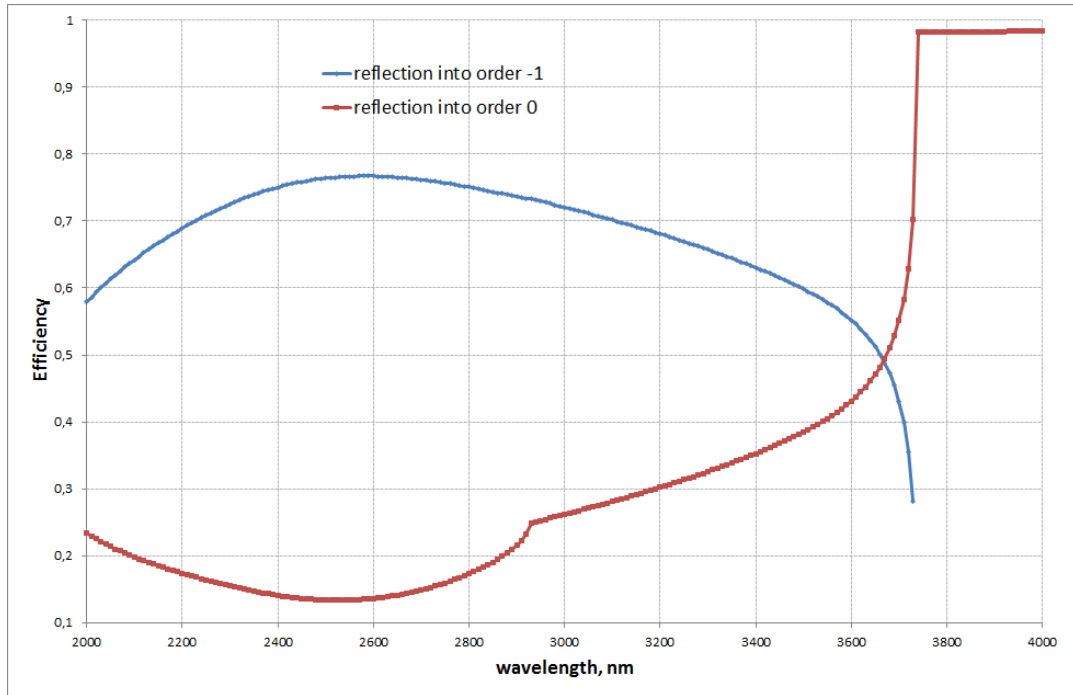


Figure 7: Efficiency spectrum of G2 with system parameters from table 2

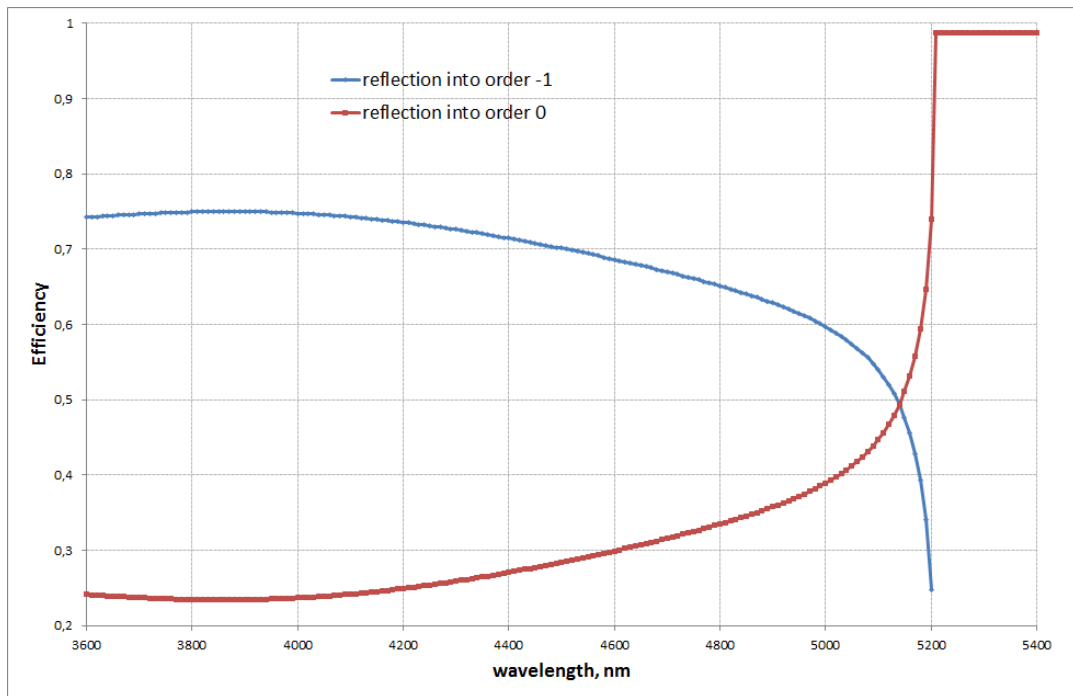


Figure 8: Efficiency spectrum of G3 with system parameters from table 2

The efficiency spectra of G1 through G3 confirm their applicability for our purpose as they feature efficiencies above 50% over the entire particular wavelength range. An additional gain in efficiency and a sharper cutoff could be reached using s polarized TR, as visible in figures 9-11.

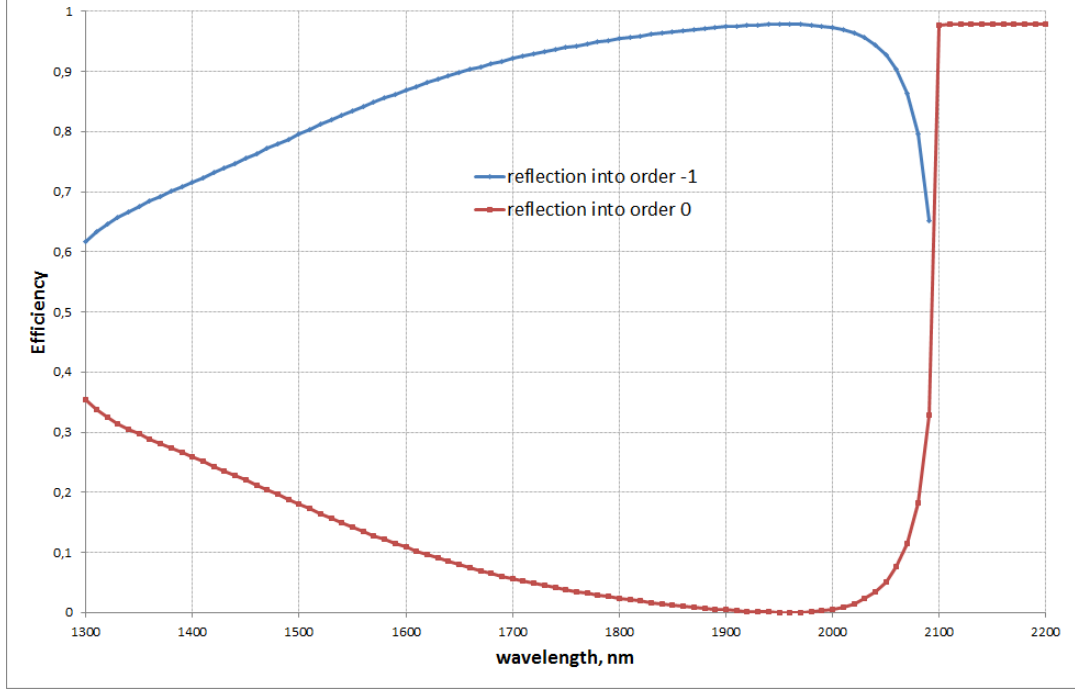


Figure 9: Efficiency spectrum of G1 with system parameters from table 2 assuming s polarized TR

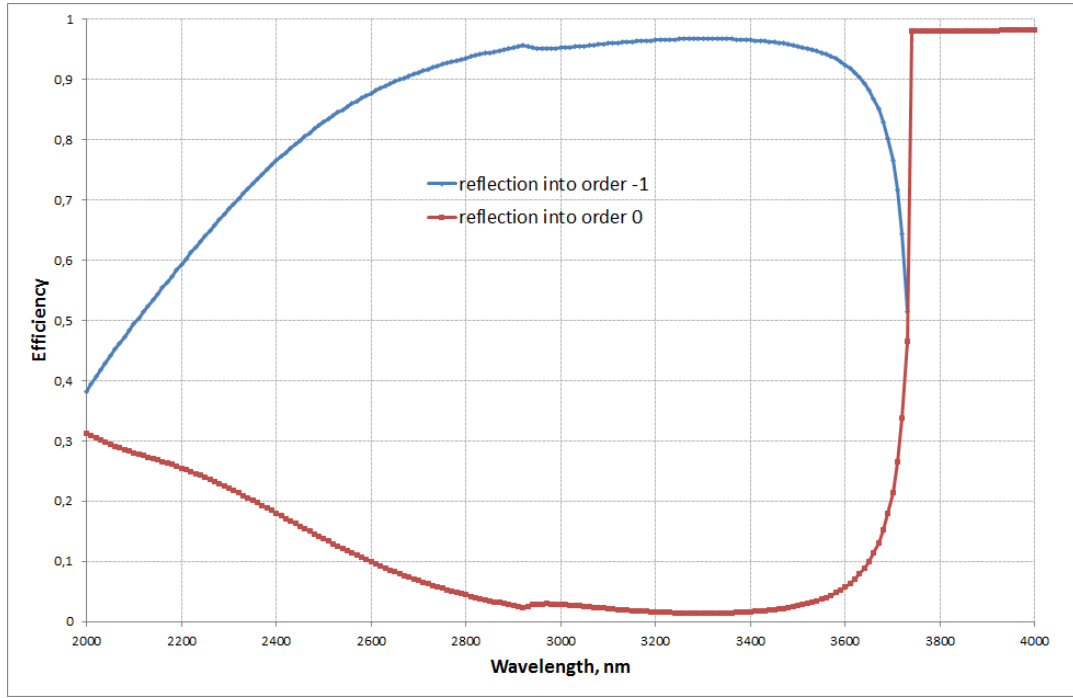


Figure 10: Efficiency spectrum of G2 with system parameters from table 2 assuming s polarized TR

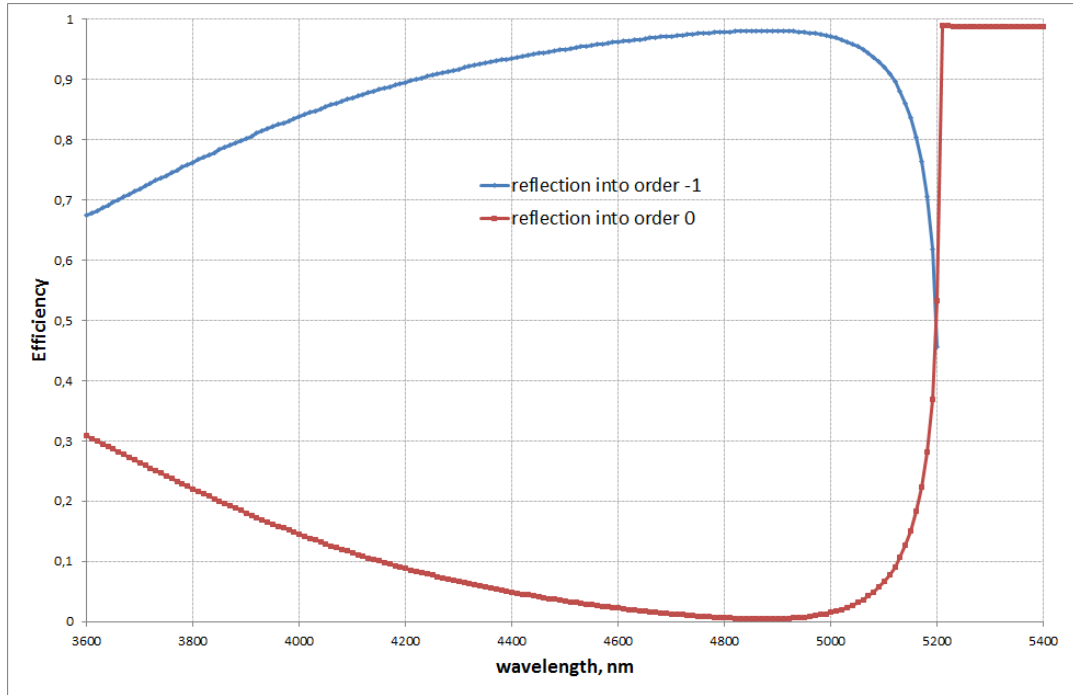


Figure 11: Efficiency spectrum of G3 with system parameters from table 2 assuming s polarized TR

However I propose not to use a polarizer as non-polarized TR leads to a flatter efficiency spectrum and the achieved efficiencies are satisfactorily high. Furthermore, the polarizer needs to be broadband and as only light featuring the desired polarisation will be transmitted to the grating, the overall TR incident on the grating would be reduced.

## 2.4 The focusing optics

There are two main challenges associated with the design of a focusing optic: The great angular range of the diffracted light and the necessity of the optic to be either transparent or reflective over the whole wavelength range. These conditions may be fulfilled using metal mirrors.

A commercially available optic to roughly focus the first order diffracted light onto a linear detector might be given by a simple parabolic mirror. Incident rays traveling parallel to the axis of revolution of a parabolic mirror are focused in one point as visible in figure 12.

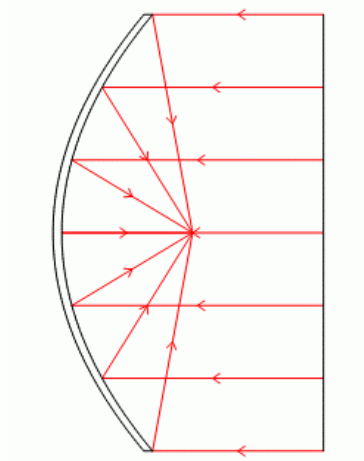


Figure 12: Collimated beam incident parallel to the axis of revolution, ray tracing performed using zemax

Simulating a tilt and decenter of a parabolic mirror on zemax, it seems to be possible to roughly align the foci of the different wavelengths. As an example, figure 13 shows a possible setup for grating G1 employing a commercial available parabolic mirror featuring a focal length  $f = 38.1 \text{ mm}$  and diameter of 2".

However, there are several problems associated with this setup.

First, collimated beams which do not travel parallel to the axis of revolution undergo distortion and coma [4] and therefore do not exactly join in a focus (figure 14).

Furthermore, the finite diameter of a monochromatic beam in x-direction (perpendicular to the plane of projection, see figure 13) needs to be considered as well. For radiation incident near the center, the shape of the mirror in x- and y-direction is roughly the same. Indeed, a collimated beam hitting the parabolic mirror at the edge discovers different mirror shapes in x- and y-direction and therefore the monochromatic collimated beam is focused at different distances in x-z- and y-z-plane. This effect can be observed in figure 15 which shows the spots of the beams on the InGaAs detector.

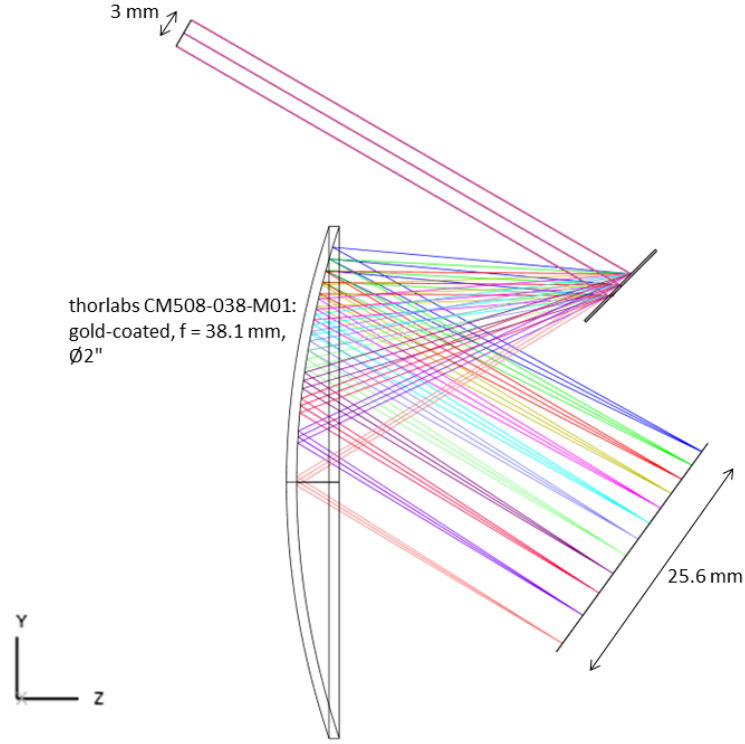


Figure 13: Cross section of G1 setup with parabolic mirror

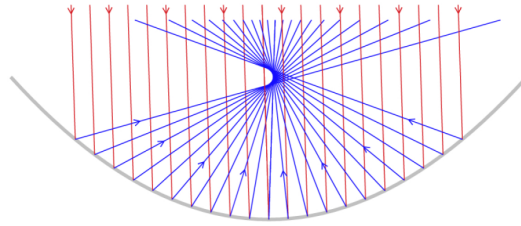


Figure 14: Collimated beam incident non-parallel to the axis of revolution [4]

Alternatively to the rough focusing by use of parabolic mirrors, an accurate focusing may be reached employing parabolic ring mirrors. Further information on their design is given in [1, 7].



Figure 15: Spot diagram at the detector position for G1 setup

### 3 Two-stage prism spectrometer: Characterization of beam splitters and measurement of visible and near-infrared TR

At present, it is not possible to perform measurements with CRISP4 and the double-prism spectrometer at the same time as this requires the placement of a beam splitter at the beginning of the setup. A further extension of the combined spectrometer by adding the two-stage prism spectrometer would demand the placement of a second beam splitter as visible in figure 16.

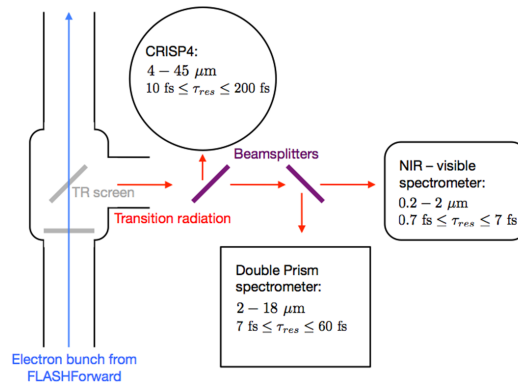


Figure 16: Setup of a broadband spectrometer combining CRISP4, the double-prism spectrometer and the two-stage prism spectrometer [6]

To approach this goal, the two-stage prism spectrometer is designed to allow the characterization of plate beam splitters in the visible and near-infrared. As different beam splitters may possess different thicknesses, the transmitted beam may be shifted due to exchange of the beam splitter. To readjust the beam path, mirror M2 can be slid back-and forwards (figure 4).

### 3.1 Choice of prisms and setup parameters

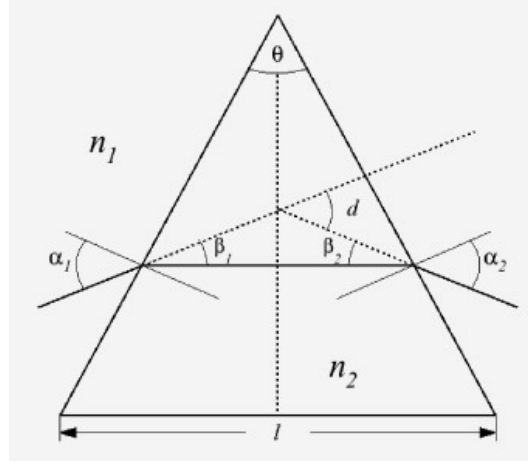


Figure 17: Cross section through a prism [10]

The deviation angle  $\delta$  of light propagating through a prism is determined by its angle of incidence  $\alpha_1$ , its wavelength  $\lambda$  and the apex angle of the prism  $\Theta$ . From figure 17, one can deduct:

$$\delta = \alpha_1 - \Theta + \arcsin(\eta_2(\lambda)) \times \sin(\Theta - \arcsin(\frac{\sin(\alpha_1)}{\eta_1(\lambda)})) \quad (6)$$

The design of the prisms is challenging as the prism material should be chosen to achieve similar deviation angle ranges  $\Delta\delta$  for similar wavelength ranges  $\Delta\lambda$ . Restricting oneself to equilateral prisms, the angle of incidence  $\alpha$  determines the overall deviation angle. Following the suggestions of M. Bornholdt [3], a  $N - SF11$  prism is employed for the near-infrared part of the spectrum and a  $CaF_2$  prism is applied for the visible light.

As the incident TR possesses a non-zero diameter, the monochromatic parallel rays need to be focused on the detector plane to achieve higher spectral resolution. Two  $N - BK7$  plano-convex lenses featuring a focal length  $f = 150 \text{ mm}$  are present. As figure 18 shows, the focal length depends on the wavelength.

For the visible part of the spectrum, a pco.edge 5.5 with a spectral range of  $0.37 - 1.1 \mu\text{m}$  is employed. The sensor contains  $2560 \times 2160$  pixels with each pixel having a length



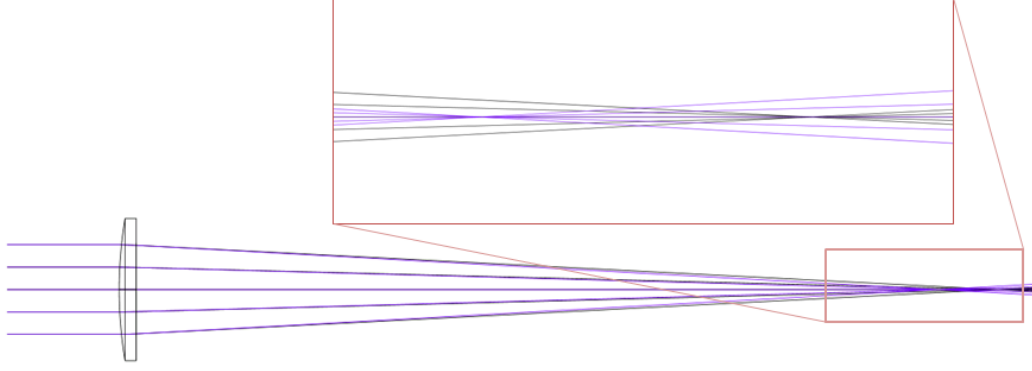


Figure 18: Cross section through a N-BK7 plano-convex lense, ray tracing performed on zemax

of  $6.5 \mu m$ . Therefore, the foci should be located on a line with a maximal length of  $l = 16.6 mm$ .

For the near-infrared measurements, an Andor iDus InGaAs 1.7 detector is available. It possesses quantum efficiencies higher than 10% over the wavelength range  $0.7 - 1.7 \mu m$ . The present detector features an array size of  $l = 12.8 mm$  containing 512 pixels.

Table 3 resumes the design parameters.

part	$\lambda [\mu m]$	prism material	lens material	$f [mm]$	$l [mm]$
visible	0.35 - 1	$CaF_2$	$N - BK7$	150	16.6
near-infrared	0.7 - 1.7	$N - SF11$	$N - BK7$	150	12.8

Table 3: Design parameters of the two-stage prism spectrometer

In order to determine the angle of incidence on the prism  $\alpha$ , distance  $d$  between prism and lens and detector tilt  $\gamma$ , the sequences containing prism, lens and detector are imaged using zemax. The three parameters are adapted so that the spectrum spreads over the entire detector surface at a small detector tilt. Furthermore,  $d$  should be greater than  $1.5 cm$  due to the size of prism and lens mounting. The optimization results are shown in figures 19 and 20.

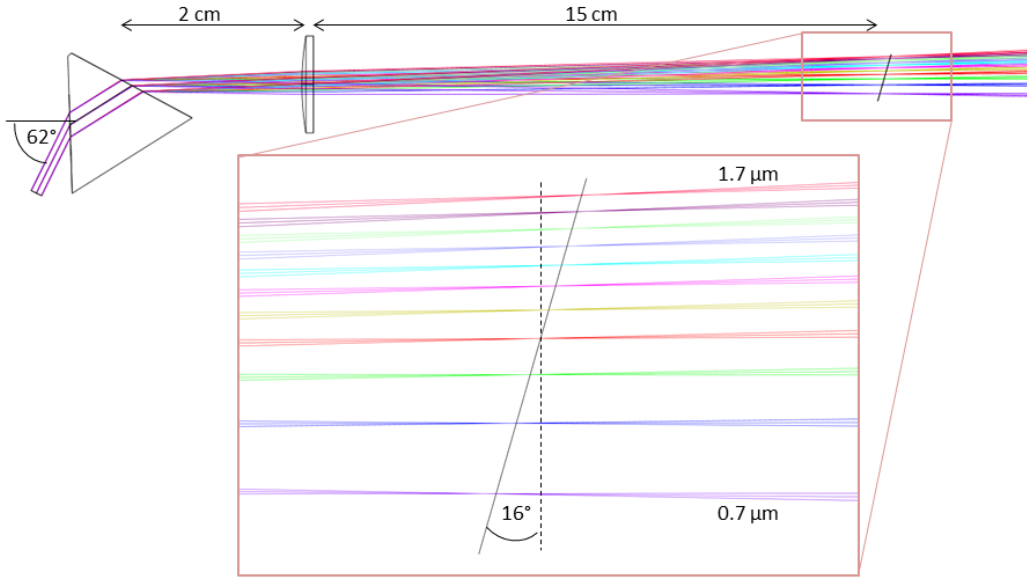


Figure 19: Prism setup for the near-infrared. Diameter of incident beam 3 mm and plotted wavelength range: 0.7 – 1.7  $\mu\text{m}$  in steps of 0.1  $\mu\text{m}$ , black line has a length of 12.8 mm

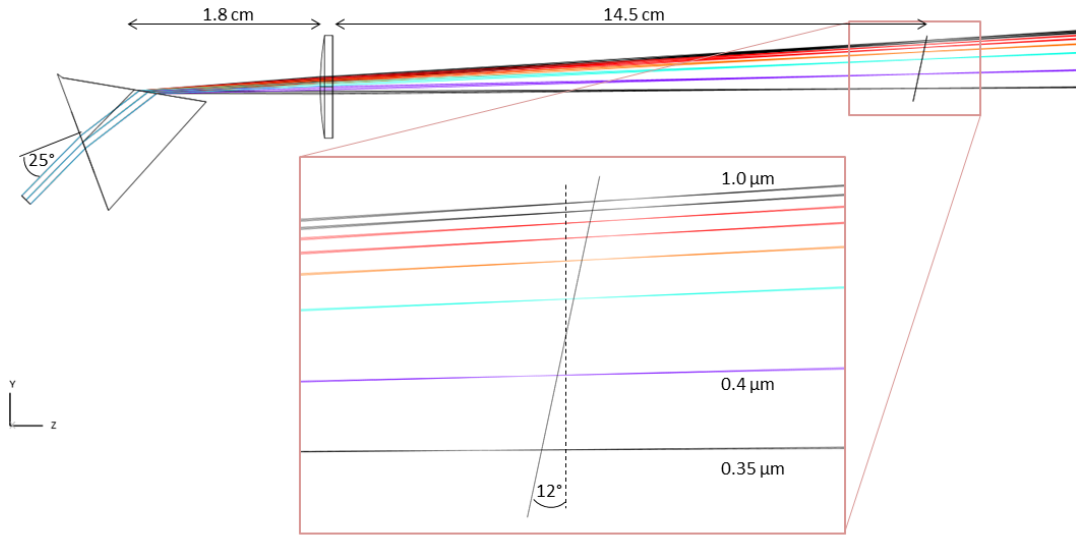


Figure 20: Prism setup for the visible. Diameter of incident beam 3 mm and plotted wavelength range: 0.35 – 1.0  $\mu\text{m}$  in steps of 0.1  $\mu\text{m}$  above 0.4  $\mu\text{m}$ , black line has a length of 16.6 mm

## 3.2 Alignment of the two-stage prism spectrometer

The setup of mirrors M1-M9 has already been realized by M. Bornholdt. For the alignment of the prisms and lenses, a 532 *nm* alignment laser is employed.

The prism mounts possess a bracket slice so that the desired angle of incidence  $\alpha$  can be set when the 0°-position is known. This position can be found looking at the reflection on the prism front surface. If the laser is normally incident, the reflected light should be sent back into the direction of incidence. By means of a piece of paper perforated with a small hole, the reflection generated by the prism is observed and the prism is rotated until incident beam and reflection overlap. The angle is read off and a rotation about the desired  $\alpha$  is carried out. By applying this method the error in the angle of incidence is reduced to the 1° level.

The alignment of the lens is more challenging. In the setup for the near-infrared, the green laser cannot be used as its wavelength is shorter than the spectrum intended to be observed. This alignment will utilize a *TiSa* oscillator beam.

For the visible setup, the green beam is not situated in the very middle of the spectrum. However, as dispersion at the position of the lens is such that the wavelengths of interest cover a region of 4.3 *mm*, with the green beam being about 1 *mm* out of center, the lens tilt and centering are adjusted with the green laser. It is planned to confirm the accuracy of the lens alignment in a subsequent step using the spectrum corresponding to a source of visible, polychromatic light on the detector.

To achieve the adjustment in height, I made use of an aperture which I fixed at a distance of a few *cm* from the prism in such a way that the beam precisely passes through. Then I placed the lens in between at the desired distance from the prism. The height of the lens is varied until the beam propagating through reaches the aperture height at the aperture position.

The lens plane is perpendicular to the axis of propagation of the green beam and the green beam passes through the center of the lens in horizontal direction if the light reflected on the front surface of the lens coincides with the incident beam and the light transmitted by the lens coincides with the aperture. These conditions are therefore fulfilled by gently tilting the lens and moving it sideways.

Concerning the detector, an additional bracket slice would allow to adjust the tilt. At present, the detector is positioned very approximately. The detector is movable on a stage which is oriented along the axis of propagation of the green beam. This will allow the variation of the detector distance remotely to adjust the imaging even during measurements with TR.

## 3.3 Wavelength calibration

For wavelength calibration, mercury, neon, xenon and argon gas lamps are available. I propose to use the mercury and neon light source to calibrate the pco.edge 5.5 camera,

as their spectra possess several discrete lines in the spectral region of interest of this branch of the spectrometer.

As the lamps do not provide a collimated beam, it is necessary to extend the prism setup by a slit and a lens. This slit is inserted between mirror M8 and prism P2 (figures 4, 21) and the centering is checked regarding the green beam on the detector. Between slit and prism, a lens is mounted so that the slit is situated in its focal plane and a collimated beam is obtained. The adjustment of the lens centering and tilt is realized analogous to the adjustment of the N-BK7 lens.

The whole optic sequence from slit to detector is finally covered with foil to shield the setup from background light originating from the gas lamp and the surroundings.

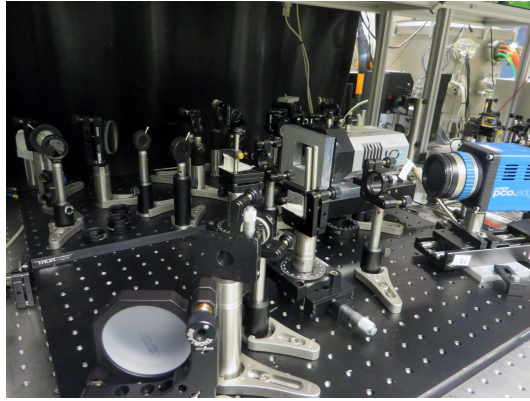


Figure 21: Setup of the two-stage prism spectrometer

## 4 Further work

Concerning the two-stage prism spectrometer, as a next step, alignment and calibration should be completed. Using a broadband light source, the spectrometer and different available beam splitters such as a hot mirror, a polka dot mirror, an ITO coated glass plate and a silicon wafer may be characterized. Finally, the detector stages may be mechanized and tests with transition radiation may be performed.

Furthermore, the extension of the present spectrometers by use of additional grating stages may be desirable. In order to extend CRISP4, the three consecutive grating stages presented in table 2 may be ordered and mounted. Alternatively, grating G1 may also be appropriate for an extension of the double-prism spectrometer down to  $1.5 \mu\text{m}$ .

As an ultimate goal, the three spectrometers may be combined into one spectrometer covering  $0.35 - 44 \mu\text{m}$  by use of adequate beam splitters.

## 5 Appendix: A brief guide to zemax

There are mainly two windows of interest: The “Lens data editor” for data input and the graphical output window accessible via “Analyze”. Before starting a simulation, one has to decide whether to work in sequential or non-sequential mode.

In sequential mode, all rays must travel through a sequence of surfaces in a given order. In non-sequential mode, this order is not predefined. Whether a ray hits the object at all depends on its position relative to the rays. Non-sequential mode should for example be applied when rays need to propagate an object several times. For my purposes, sequential mode was employed.

Before starting to design an optic, one should consult the producer homepage as there may be a zemax file available. In addition, one should have a look into the knowledgebase provided on the zemax homepage. Some files for more complex optics and corresponding explanation documents are available there. Having a look at some of the provided files may also be appropriate as examples for the first tries on zemax. A description of all predefined surfaces is given in the zemax manual.

As zemax does not provide many error messages, the order of implementing the optics on zemax should follow the path of the light and one should check the beam path after each new component.

## References

- [1] S.Wesch et al., *A Multi-Channel THz and Infrared Spectrometer for Femtosecond Electron Bunch Diagnostics by Single-Shot Spectroscopy of Coherent Radiation*, Nuclear Instruments and Methods A (2012).
- [2] S. Wunderlich et al., *A double-prism spectrometer for the longitudinal diagnosis of femtosecond electron bunches with mid-infrared transition radiation*, IBIC (2014).
- [3] M. Bornholdt, *private communication*.
- [4] A. April et al., *Focusing a TM01 beam with a slightly tilted parabolic mirror*, Optics Express (2011).
- [5] J. Osterhoff et al., *Controlled Electron-Beam Injection into Plasma Waves for Tailored Betatron-Radiation Generation*, GCS (2015).
- [6] C. Palmer, *private communication*.
- [7] S. Wesch, *Echtzeitbestimmung longitudinaler Elektronenstrahlparameter mittels absoluter Intensitäts- und Spektralmessung einzelner kohärenter THz Strahlungspulse*, DESY-THESIS-2012-052 (2012).
- [8] O. Grimm, P. Schmüser, *Principles of longitudinal beam diagnostics with coherent radiation*, TESLA-FEL–2006-03 (2006).
- [9] N. Neumann, *Pyroelektrische Detektoren füßr die Infrarot-Gasanalytik*, Sensor Magazin 4/2012, p. 20-21.
- [10] I. Yeo et al., *Measurement of the refractive index of the LAB-based liquid scintillator and acrylic at RENO*, Physica Scripta, Volume 82, Number 6 (2010).